3D relativistic Hartree-Bogoliubov model with a separable pairing interaction: Triaxial ground-state shapes

Nikšić, Tamara; Ring, Peter; Vretenar, Dario; Tian, Yuan; Ma, Zhong-yu

3D relativistic Hartree-Bogoliubov model with a separable pairing interaction: Triaxial ground-state shapes

T. Nikšić

Physics Department, Faculty of Science, University of Zagreb, HR-10000 Zagreb, Croatia

P. Ring and D. Vretenar

Physik Department der Technischen Universität München, D-85748 Garching, Germany

Yuan Tian and Zhong-yu Ma

China Institute of Atomic Energy, Beijing 102413, People's Republic of China

Potential-energy surfaces and pairing energy maps of nuclei with triaxial shapes are studied in the framework of the relativistic Hartree-Bogoliubov (RHB) model. The recently introduced separable pairing force, adjusted in nuclear matter to the pairing gap of the Gogny force, is employed in the pairing channel of the three-dimensional RHB model for triaxial shapes, and the density-dependent meson-exchange effective interaction (DD-ME2) is used in the particle-hole channel. Even-*A* Pt isotopes with triaxial ground-state shapes and Sm nuclei with γ-soft potential-energy surfaces are analyzed.

I. INTRODUCTION

The structure of heavy complex nuclei with a large number of active valence nucleons is, at present, best described by the framework of nuclear energy density functionals (NEDF). A variety of structure phenomena, not only in stable nuclei, but also in regions of nuclei far from the valley of β stability and close to the nucleon drip lines, have been described with self-consistent mean-field models based on the Gogny interaction, the Skyrme energy functional, and the relativistic meson-exchange effective Lagrangians [1,2].

Self-consistent relativistic mean-field (RMF) models have been employed in analyses of properties of ground and excited states in spherical and deformed nuclei. For a quantitative analysis of open-shell nuclei it is also necessary to consider pairing correlations. Pairing has often been taken into account in a very phenomenological way in the BCS model with the monopole pairing force, adjusted to the experimental odd-even mass differences. In many cases, however, this approach presents only a poor approximation. The physics of weakly bound nuclei, in particular, necessitates a unified and self-consistent treatment of mean-field and pairing correlations. This has led to the formulation and development of the relativistic Hartree-Bogoliubov (RHB) model [3], which represents a relativistic extension of the conventional Hartree-Fock-Bogoliubov framework. In most applications of the RHB model [2] the pairing part of the Gogny force [4] has be employed in the particle-particle (pp) channel

$$V^{pp}(1, 2) = \sum_{i=1,2} e^{-[(\mathbf{r}_1-\mathbf{r}_2)/\mu_i]^2}$$
$$\times (W_i + B_i P^\sigma - H_i P^\tau - M_i P^\sigma P^\tau), \quad (1)$$

with the set D1S [5] for the parameters μ_i, W_i, B_i, H_i, and M_i ($i = 1, 2$). A basic advantage of the Gogny force is the finite range, which automatically guarantees a proper cutoff in momentum space. However, the resulting pairing field is nonlocal and the solution of the corresponding Dirac-Hartree-Bogoliubov integro-differential equations can be time consuming, especially in the case of three-dimensional (3D) calculations for nuclei with triaxial shapes. An alternative is the use of a zero-range, possibly density-dependent, δ force in the pp channel of the RHB model [6], but this approach introduces an additional cutoff parameter in energy. The effective range of the pairing interaction is determined by the energy cutoff, and the strength parameter must be chosen accordingly in order to reproduce empirical pairing gaps. In Ref. [7] we have implemented a renormalization scheme for the relativistic Hartree-Bogoliubov equations with a zero-range pairing interaction. The procedure is equivalent to a simple energy cutoff with a position-dependent coupling constant, and the resulting average pairing gaps and pairing energies do not depend on the cutoff energy. A density-dependent strength parameter of the zero-range pairing can be adjusted in such a way that the renormalization procedure reproduces in symmetric nuclear matter the pairing gap of the Gogny force equation (1).

In a series of recent articles [8–10] we have introduced a separable form of the pairing force for RHB calculations in spherical and axially deformed nuclei. The force is separable in momentum space, and is completely determined by two parameters that are adjusted to reproduce in symmetric nuclear matter the bell-shape curve of the pairing gap of the Gogny force. In applications to finite nuclei, when transformed from momentum to coordinate space, this pairing force is no longer separable because of translational invariance. It has been shown, however, that a method developed by Talmi and Moshinsky can be used to represent the corresponding pp matrix elements as a sum of a finite number of separable terms. When the nucleon wave functions are expanded in a harmonic-oscillator basis, spherical or axially deformed, the sum converges relatively quickly (i.e., a reasonably small number of separable terms reproduce with high accuracy the results of calculations performed in a complete basis). The simple separable force considered in Refs. [8–10] reproduces pairing properties of spherical and axially deformed nuclei

calculated with the original Gogny force, but with the important advantage that the computational cost is greatly reduced.

In the present work we extend the model to the calculation of energy surfaces of nuclei with triaxial shapes. The three-dimensionsl (3D) RHB model with a separable pairing interaction in the pp channel enables very efficient systematic calculations of RHB binding-energy surfaces in the β-γ plane, based on relativistic nuclear energy density functionals, that can eventually be used as input for the generator coordinate method configuration mixing of angular momentum projected triaxial wave functions, or to determine the parameters of a five-dimensional collective Hamiltonian for quadrupole vibrational and rotational degrees of freedom [11]. In Sec. II we introduce the 3D RHB model and derive the pp matrix element of the pairing force as a sum of a finite number of separable terms in the basis of a 3D harmonic oscillator. Illustrative calculations for even-A Sm and Pt isotopes are presented in Sec. III. Section IV summarizes the results and ends with an outlook for future applications. Details on the expansion of single-nucleon spinors in the 3D harmonic-oscillator basis, the transformation of the product of harmonic-oscillator wave functions to the center-of-mass frame, and calculation of pairing matrix elements, are included in Appendixes A–C.

II. 3D RELATIVISTIC HARTREE-BOGOLIUBOV MODEL WITH A SEPARABLE PAIRING INTERACTION

The relativistic Hartree-Bogoliubov framework [2] provides a unified description of ph and particle-particle pp correlations on a mean-field level by using two average potentials: the self-consistent mean field that encloses all the long-range ph correlations, and a pairing field $\hat{\Delta}$ which sums up the pp correlations. The ground state of a nucleus is described by a generalized Slater determinant $|\Phi\rangle$ that represents the vacuum with respect to independent quasiparticles. The quasiparticle operators are defined by the unitary Bogoliubov transformation of the single-nucleon creation and annihilation operators,

$$\alpha_k^+ = \sum_l U_{lk} c_l^+ + V_{lk} c_l, \tag{2}$$

where U and V are the Hartree-Bogoliubov wave functions determined by the solution of the RHB equation. In coordinate representation

$$\begin{pmatrix} h_D - m - \lambda & \Delta \\ -\Delta^* & -h_D^* + m + \lambda \end{pmatrix} \begin{pmatrix} U_k(\boldsymbol{r}) \\ V_k(\boldsymbol{r}) \end{pmatrix} = E_k \begin{pmatrix} U_k(\boldsymbol{r}) \\ V_k(\boldsymbol{r}) \end{pmatrix}. \tag{3}$$

In the relativistic case the self-consistent mean field corresponds to the single-nucleon Dirac Hamiltonian $\hat{h}_D$. In the usual σ, ω, and ρ meson-exchange representation, and for the stationary case with time-reversal symmetry (i.e., for the ground-state of an even-even nucleus),

$$\hat{h}_D = -i\boldsymbol{\alpha}\boldsymbol{\nabla} + \beta[m + g_\sigma \sigma(\boldsymbol{r})] + g_\omega \omega^0(\boldsymbol{r})$$
$$+ g_\rho \tau_3 \rho^0(\boldsymbol{r}) + e\frac{1-\tau_3}{2} A^0(\boldsymbol{r}). \tag{4}$$

The classical meson fields are solutions of the stationary Klein-Gordon equations:

$$(-\triangle + m_\sigma^2)\sigma(\boldsymbol{r}) = -g_\sigma(\rho)\rho_s(\boldsymbol{r}), \tag{5}$$

$$(-\triangle + m_\omega^2)\omega^0(\boldsymbol{r}) = g_\omega(\rho)\rho(\boldsymbol{r}), \tag{6}$$

$$(-\triangle + m_\rho^2)\rho^0(\boldsymbol{r}) = g_\rho(\rho)\rho_3^0(\boldsymbol{r}), \tag{7}$$

$$-\triangle A^0(\boldsymbol{r}) = \rho_p(\boldsymbol{r}), \tag{8}$$

for the σ meson, the timelike components of the ω meson and ρ meson, and the Poisson equation for the vector potential, respectively. In the general case when the meson-nucleon couplings g_σ, g_ω, and g_ρ explicitly depend on the nucleon (vector) density ρ, there is an additional contribution to the nucleon self-energy—the rearrangement term [2], essential for the energy-momentum conservation and the thermodynamical consistency of the model.

In Eq. (3) m is the nucleon mass, and the chemical potential λ is determined by the particle number subsidiary condition in order that the expectation value of the particle number operator in the ground state equals the number of nucleons. The pairing field Δ reads

$$\Delta_{ab}(\boldsymbol{r}, \boldsymbol{r}') = \frac{1}{2} \sum_{c,d} V_{abcd}(\boldsymbol{r}, \boldsymbol{r}')\kappa_{cd}(\boldsymbol{r}, \boldsymbol{r}'), \tag{9}$$

where $V_{abcd}(\boldsymbol{r}, \boldsymbol{r}')$ are the matrix elements of the two-body pairing interaction, and the indices a, b, c, and d denote the quantum numbers that specify the Dirac indices of the spinor. The column vectors denote the quasiparticle wave functions, and E_k are the quasiparticle energies. The dimension of the RHB matrix equation is two times the dimension of the corresponding Dirac equation. For each eigenvector (U_k, V_k) with positive quasiparticle energy $E_k > 0$, there exists an eigenvector (V_k^*, U_k^*) with quasiparticle energy $-E_k$. Since the baryon quasiparticle operators satisfy fermion commutation relations, the levels E_k and $-E_k$ cannot be occupied simultaneously. For the solution that corresponds to a ground state of a nucleus with an even particle number, one usually chooses the eigenvectors with positive eigenvalues E_k.

The single-particle density and the pairing tensor, constructed from the quasiparticle wave functions

$$\rho_{cd}(\boldsymbol{r}, \boldsymbol{r}') = \sum_{k>0} V_{ck}^*(\boldsymbol{r})V_{dk}(\boldsymbol{r}'), \tag{10}$$

$$\kappa_{cd}(\boldsymbol{r}, \boldsymbol{r}') = \sum_{k>0} U_{ck}^*(\boldsymbol{r})V_{dk}(\boldsymbol{r}'), \tag{11}$$

are calculated in the *no-sea* approximation (denoted by $k > 0$): the summation runs over all quasiparticle states k with positive quasiparticle energies $E_k > 0$ but omits states that originate from the Dirac sea. The latter are characterized by a quasiparticle energy larger than the Dirac gap ($\approx$1200 MeV).

Pairing correlations in nuclei are restricted to an energy window of a few MeV around the Fermi level, and their scale is well separated from the scale of binding energies, which are in the range of several hundred to a thousand MeV. There is no empirical evidence for any relativistic effect in the nuclear pairing field $\hat{\Delta}$ and, therefore, a hybrid RHB model with a nonrelativistic pairing interaction can be formulated.

For a general two-body interaction, the matrix elements of the relativistic pairing field read

$$\hat{\Delta}_{a_1 p_1, a_2 p_2} = \frac{1}{2} \sum_{a_3 p_3, a_4 p_4} \langle a_1 p_1, a_2 p_2 | V^{pp} \\ \times |a_3 p_3, a_4 p_4 \rangle_a \kappa_{a_3 p_3, a_4 p_4}, \quad (12)$$

where the indices ($p_1, p_2, p_3, p_4 \equiv f, g$) refer to the large and small components of the quasiparticle Dirac spinors:

$$U(\mathbf{r}, s, t) = \begin{pmatrix} f_U(\mathbf{r}, s, t) \\ i g_U(\mathbf{r}, s, t) \end{pmatrix}, \quad V(\mathbf{r}, s, t) = \begin{pmatrix} f_V(\mathbf{r}, s, t) \\ i g_V(\mathbf{r}, s, t) \end{pmatrix}. \quad (13)$$

In practical applications of the RHB model to finite open-shell nuclei, only the large components of the spinors $U_k(\mathbf{r})$ and $V_k(\mathbf{r})$ are used to build the nonrelativistic pairing tensor $\hat{\kappa}$ in Eq. (10). The resulting pairing field reads

$$\hat{\Delta}_{a_1 f, a_2 f} = \frac{1}{2} \sum_{a_3 f, a_4 f} \langle a_1 f, a_2 f | V^{pp} | a_3 f, a_4 f \rangle_a \kappa_{a_3 f, a_4 f}. \quad (14)$$

The other components, $\hat{\Delta}_{fg}$, $\hat{\Delta}_{gf}$, and $\hat{\Delta}_{gg}$, can be safely omitted [12].

The Dirac-Hartree-Bogoliubov equations and the equations for the meson fields are solved by expanding the nucleon spinors $U(\mathbf{r}, s, t)$ and $V(\mathbf{r}, s, t)$, and the meson fields, in the basis of a three-dimensional harmonic oscillator (HO) in Cartesian coordinates. In this way both axial and triaxial nuclear shapes can be described. In addition, to reduce the computational task, it is assumed that the total densities are symmetric under reflections with respect to all three planes xy, xz, and yz. When combined with time-reversal invariance, this also implies that parity is conserved. The single-nucleon basis is defined in Appendix A.

In Ref. [8] a new separable form of the pairing interaction has been introduced, with parameters adjusted to reproduce the pairing properties of the Gogny force in nuclear matter. The gap equation in the $^1S_0$ channel reads

$$\Delta(k) = -\int_0^\infty \frac{k'^2 dk'}{2\pi^2} \langle k | V^{1S_0} | k' \rangle \frac{\Delta(k')}{2E(k')}, \quad (15)$$

and the pairing force is separable in momentum space,

$$\langle k | V^{1S_0} | k' \rangle = -G p(k) p(k'). \quad (16)$$

By assuming a simple Gaussian ansatz $p(k) = e^{-a^2 k^2}$, the two parameters G and a have been adjusted to reproduce the density dependence of the gap at the Fermi surface, calculated with a Gogny force. For the D1S parametrization [5] of the Gogny force: $G = -728$ MeVfm^3 and $a = 0.644$ fm. When the pairing force Eq. (16) is transformed from momentum to coordinate space, it takes the form

$$V(\mathbf{r}_1, \mathbf{r}_2, \mathbf{r}'_1, \mathbf{r}'_2) = G \delta(\mathbf{R} - \mathbf{R}') P(\mathbf{r}) P(\mathbf{r}') \frac{1}{2} (1 - P^\sigma), \quad (17)$$

where $\mathbf{R} = \frac{1}{2}(\mathbf{r}_1 + \mathbf{r}_2)$ and $\mathbf{r} = \mathbf{r}_1 - \mathbf{r}_2$ denote the center of mass and the relative coordinates, and $P(\mathbf{r})$ is the Fourier transform of $p(k)$,

$$P(\mathbf{r}) = \frac{1}{(4\pi a^2)^{3/2}} e^{-r^2/4a^2}. \quad (18)$$

The pairing force has finite range and, because of the presence of the factor $\delta(\mathbf{R} - \mathbf{R}')$, it preserves translational invariance. Even though $\delta(\mathbf{R} - \mathbf{R}')$ implies that this force is not completely separable in coordinate space, the corresponding antisymmetrized pp matrix elements

$$\langle \alpha \bar{\beta} | V | \gamma \bar{\delta} \rangle_a = \langle \alpha \bar{\beta} | V | \gamma \bar{\delta} \rangle - \langle \alpha \bar{\beta} | V | \bar{\delta} \gamma \rangle, \quad (19)$$

can be represented as a sum of a finite number of separable terms in the basis of a 3D harmonic oscillator (see Appendix C for details):

$$\langle \alpha \bar{\beta} | V | \gamma \bar{\delta} \rangle_a = G \sum_{N_x=0}^{N_x^0} \sum_{N_y=0}^{N_y^0} \sum_{N_z=0}^{N_z^0} \left(V_{\alpha\bar{\beta}}^{N_x N_y N_z} \right)^* V_{\gamma\bar{\delta}}^{N_x N_y N_z}, \quad (20)$$

where N_x, N_y, and N_z are the quantum numbers of the corresponding one-dimensional (1D) HO's in the center-of-mass frame (cf. Appendix B). This means that the pairing field can also be written as a sum of a finite number of separable terms

$$\Delta_{\alpha\bar{\beta}} = G \sum_{N_x=0}^{N_x^0} \sum_{N_y=0}^{N_y^0} \sum_{N_z=0}^{N_z^0} \left(V_{\alpha\bar{\beta}}^{N_x N_y N_z} \right)^* P_{N_x N_y N_z}, \quad (21)$$

with the coefficients

$$P_{N_x N_y N_z} = \sum_{\gamma\delta>0} V_{\gamma\bar{\delta}}^{N_x N_y N_z} \kappa_{\gamma\bar{\delta}}. \quad (22)$$

The advantage of using the separable pairing interaction Eq. (17) is that the matrices $V_{\alpha\bar{\beta}}^{N_x N_y N_z}$ are calculated only once at the beginning of a self-consistent calculation [the explicit expression in a 3D Cartesian oscillator basis for which is given by Eq. (C15)]. The coefficients $P_{N_x N_y N_z}$ are recalculated at each iteration step, using the corresponding updated pairing tensor κ.

The number of terms in Eqs. (20) and (21) is, in principle, limited by the dimension of the oscillator basis. If single-particle oscillator states $|n_x n_y n_z\rangle$ with $n_x + n_y + n_z \leqslant N_f^{\max}$ form the basis, the summation over the quantum number of the 1D HO in the center-of-mass frame in Eq. (C7) runs over $N_x = 0, \ldots, 2N_f^{\max}$. This means that the maximal total number of terms in Eqs. (20) and (21) equals $N_{\text{tot}}^{\max} = (2N_f^{\max} + 1)^3$. However, results of calculations performed in Refs. [8,10] suggest that the actual number of terms that give significant contributions to the pairing field is much smaller. If a cutoff condition is imposed

$$N_x \leqslant N_x^c, \quad N_y \leqslant N_y^c, \quad N_z \leqslant N_z^c, \quad (23)$$

the total number of separable terms becomes

$$N_{\text{sep}} = \frac{1}{8} (N_x^c + 2)(N_y^c + 2)(N_z^c + 2). \quad (24)$$

In the next section we will compare some results of illustrative 3D RHB calculations with those obtained assuming axial symmetry [10]. For a meaningful comparison with results calculated using the axial RHBZ code [10], we will make the following choice: $N_x + N_y \leqslant N_\perp^c$ and $N_z \leqslant N_z^c$. In this case the total number of separable terms equals

$$N_{\text{sep}}^{\text{axial}} = \frac{1}{8} (N_\perp^c + 1)^2 (N_z^c + 2). \quad (25)$$

III. ILLUSTRATIVE CALCULATIONS

In this section we present the results of illustrative 3D RHB calculations for two cases: a sequence of γ-soft Sm nuclei and a chain of Pt isotopes that display minima in the γ plane. The separable pairing force Eq. (17) is used in the pp channel, and the mean field is determined by the density-dependent meson-exchange effective interaction (DD-ME2) [13] in the ph channel. DD-ME2 has been adjusted to empirical properties of symmetric and asymmetric nuclear matter, binding energies, charge radii, and neutron radii of spherical nuclei. The interaction has been tested in calculations of ground-state properties of a large set of spherical and deformed nuclei. An excellent agreement with data has been obtained for binding energies, charge isotope shifts, and quadrupole deformations. When used in the relativistic random-phase approximation (RPA), DD-ME2 reproduces with high accuracy data on isoscalar and isovector collective excitations [13,14].

A. Ground-state shapes of Sm isotopes

In Figs. 1 and 2 we display the self-consistent RHB triaxial quadrupole binding-energy maps of the $^{134-156}$Sm isotopes in the β-γ plane ($0° \leqslant \gamma \leqslant 60°$). The map of the energy surface as a function of the quadrupole deformation is obtained by imposing constraints on the axial and triaxial quadrupole moments. The method of quadratic constraint uses an unrestricted variation of the function

$$\langle \hat{H} \rangle + \sum_{\mu=0,2} C_{2\mu}(\langle \hat{Q}_{2\mu} \rangle - q_{2\mu})^2, \qquad (26)$$

where $\langle \hat{H} \rangle$ is the total energy and $\langle \hat{Q}_{2\mu} \rangle$ denotes the expectation value of the mass quadrupole operators

$$\hat{Q}_{20} = 2z^2 - x^2 - y^2 \quad \text{and} \quad \hat{Q}_{22} = x^2 - y^2. \qquad (27)$$

$q_{2\mu}$ is the constrained value of the multipole moment and $C_{2\mu}$ the corresponding stiffness constant [15].

The energy maps shown in Figs. 1 and 2 nicely illustrate the gradual transition from the prolate and γ-soft deformed light isotopes ^{134,136}Sm, through the spherical $N = 82$ neutron closed-shell nucleus ^{144}Sm, to the strongly prolate deformed, axial nuclei ^{154,156}Sm. The isotopes below the $N = 82$ closed shell are all γ soft and, just before the shell closure, one finds a slightly oblate minimum in ^{140}Sm. Sm nuclei with $N > 82$ quickly develop a pronounced prolate deformation, much stiffer with respect to the γ degree of freedom than isotopes below $N = 82$. Heavy Sm isotopes are characterized by axially symmetric shapes with pronounced prolate minima at $\beta > 0.3$.

The binding-energy maps correspond to self-consistent solutions of the RHB equations, obtained by expanding the nucleon spinors and the meson fields in the basis of a three-dimensional harmonic oscillator in Cartesian coordinates. In the present calculation the basis includes $N_f^{max} = 14$ major oscillator shells. In Figs. 3 and 4 we plot the corresponding contour maps of the proton and neutron pairing energies in the β-γ plane for the three lighter isotopes ^{134,136,138}Sm, and for the three heavier nuclei ^{152,154,156}Sm, respectively. By using the separable pairing force Eq. (17), the pairing field Eq. (21)
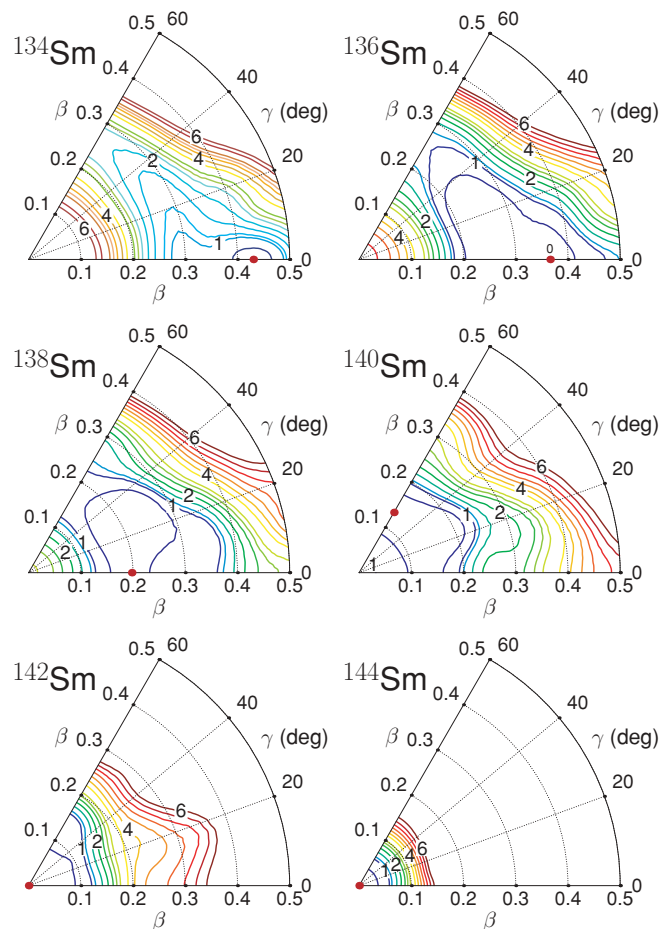

FIG. 1. (Color online) Self-consistent RHB triaxial quadrupole binding-energy maps of the even-even isotopes $^{134-144}$Sm in the $\beta-\gamma$ plane ($0 \leqslant \gamma \leqslant 60°$). All energies are normalized with respect to the binding energy of the absolute minimum (red dot). The contours join points on the surface with the same energy (in MeV).

and the pairing energy

$$E_{\text{pair}} = G \sum_{N_x=0}^{N_x^0} \sum_{N_y=0}^{N_y^0} \sum_{N_z=0}^{N_z^0} |P_{N_x N_y N_z}|^2 \qquad (28)$$

are calculated as sums of a finite number of separable terms. Because pairing energy depends on the level density at the Fermi surface for any given deformation, the plots in Figs. 3 and 4 show pronounced fluctuations that reflect the underlying shell structure. The strong fluctuations in the pairing energy are compensated to a large extent by the mean-field energy in the ph channel, leading to the much smoother total binding-energy maps shown in Figs. 1 and 2.

We have verified the 3D calculations in the pp channel by comparing the results for ground-state properties of $^{134-154}$Sm with those obtained using the axial RHBZ code with the same separable pairing force [10] and with the pairing part of the original Gogny force [5,16]. In the case when axial symmetry is assumed, the expansion for the pairing field runs over the quantum numbers N_z and N_p of the HO in the center-of-mass frame, corresponding to the z and ρ coordinates of the
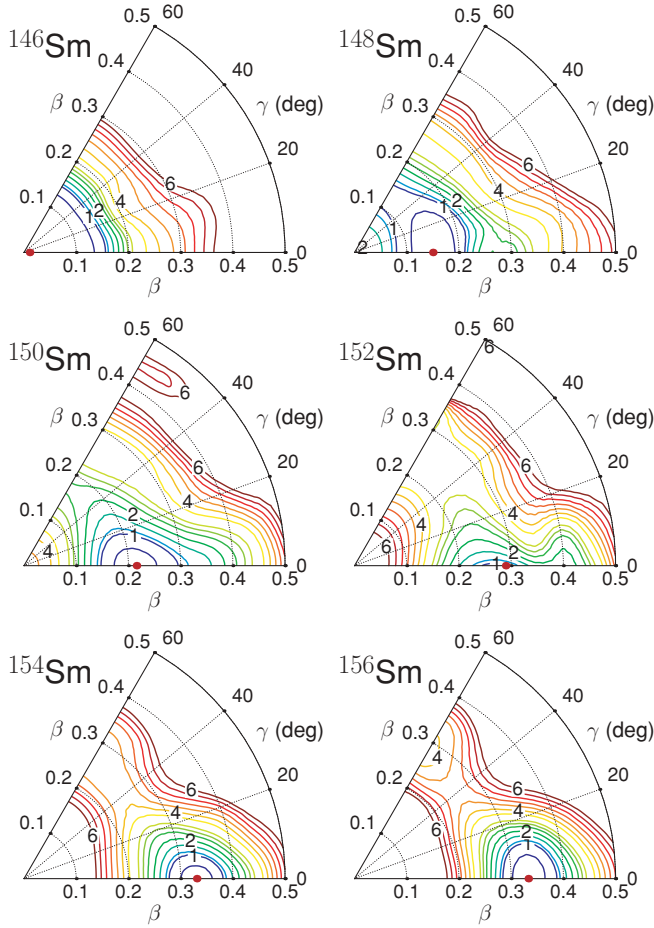
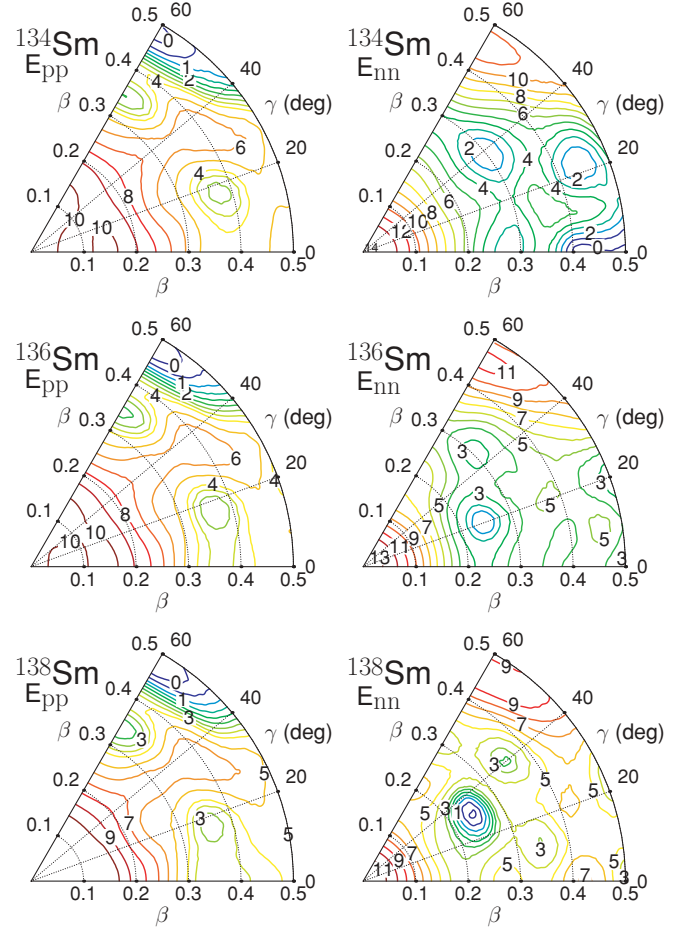FIG. 2. (Color online) Same as described in the caption to Fig. 1 but for the isotopes $^{146-156}$Sm.

FIG. 3. (Color online) Proton (left column) and neutron (right column) pairing energies $E_{pp(nn)} = -E_{\text{pair}}$ in Eq. (28) for the nuclei ^{134,136,138}Sm in the $\beta-\gamma$ plane ($0 \leqslant \gamma \leqslant 60°$). The contours join points on the surface with the same energy (in MeV).

cylindrical coordinate system,

$$\Delta_{12} = -G \sum_{N_z}^{N_z^0} \sum_{N_p}^{N_p^0} W_{12}^{N_z N_p} P_{N_z} P_{N_p}. \qquad (29)$$

The maximal values for the quantum numbers in the expansion of Dirac spinors are $n_z^0 = N_f^{\text{max}}$ and $n_p^0 = N_f^{\text{max}}/2$, i.e., the maximal values for the coefficients in expansion (29) are $N_z^0 = 2n_z^0 = 2N_f^{\text{max}}$ and $N_p^0 = 2n_p^0 = N_f^{\text{max}}$. In Ref. [10] it has been shown that for axial calculations of prolate deformed nuclei, sufficient accuracy is achieved if the expansion of pairing matrix elements is limited to $N_p \leqslant N_p^0 = 5$ and $N_z \leqslant N_z^0 = 14$. For this choice of the cutoff in the expansion of the pairing matrix elements in the basis of the HO in the center-of-mass frame, the resulting pairing energies reproduce to a very good approximation results obtained with the calculation in the full basis, and also those obtained with the Gogny force D1S in the pairing channel. In the present 3D calculation we have, therefore, imposed the following cutoff condition for the expansion in Eqs. (20), (21), and (22),

$$N_z = 0, 2, \ldots, N_z^0 = 14 \quad \text{and}$$
$$N_x + N_y = 0, 2, \ldots, 2N_p^0 = 5. \qquad (30)$$

In Fig. 5 we display the 3D RHB ground-state binding energies for the Sm isotopes ($72 \leqslant N \leqslant 92$) in comparison with data from the compilation of Audi and Wapstra [17]. Calculations have also been performed with the axial RHBZ code [10], and the inset plots the relative differences (in percent): $(E^{\text{RHBZ}} - E^{\text{3DRHB}})/E^{\text{3DRHB}}$, between the corresponding ground-state binding energies. As a further test, Fig. 6 compares the 3D RHB and axial (RHBZ) results for the self-consistent ground-sate quadrupole deformations and neutron and proton pairing energies of even-A Sm isotopes. In calculations with axial symmetry (RHBZ) both the separable force and the Gogny D1S force [5] are used in the pairing channel. The agreement between the three sets of results demonstrates not only the numerical accuracy of the new 3D computer code, but also that by using the separable pairing force in deformed nuclei, virtually identical pairing energies are calculated as with the original Gogny force.

B. Evolution of triaxial shapes in Pt isotopes

Even though a large majority of deformed nuclei display axially symmetric prolate ground-state shapes, some regions of the nuclide chart are characterized by the occurrence of oblate deformed and triaxial shapes. One of the examples is the
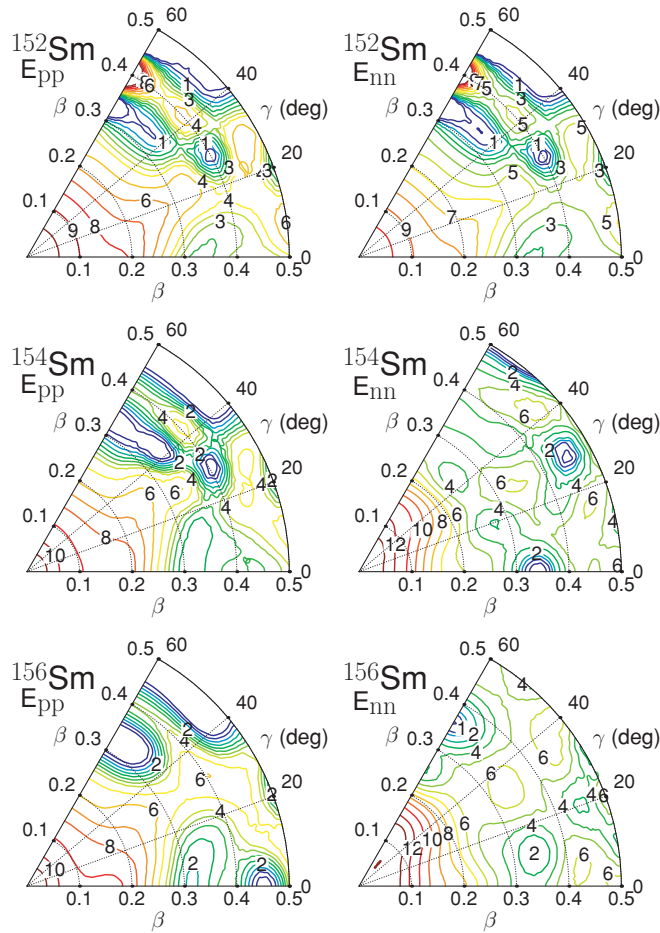
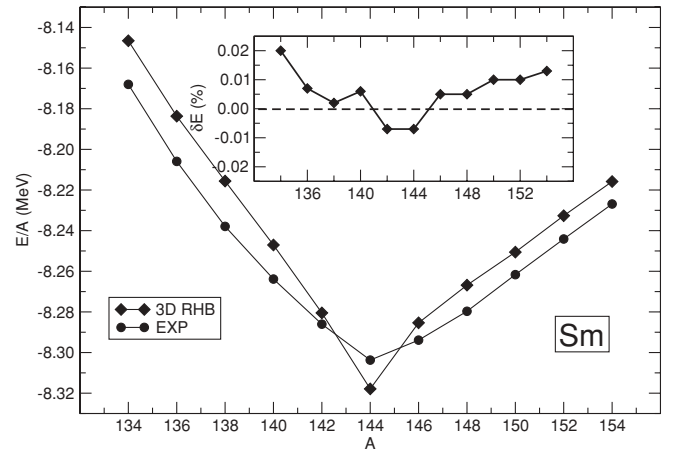FIG. 4. (Color online) Same as described in the caption to Fig. 3 but for the isotopes ^{152,154,156}Sm.

FIG. 5. Binding energy per nucleon for the sequence of Sm isotopes, calculated with the 3D RHB model and compared to data [17]. In the inset we display the relative differences (in %): $(E^{\mathrm{RHBZ}} - E^{\mathrm{3DRHB}})/E^{\mathrm{3DRHB}}$, between the binding energies calculated using the 3D RHB and the axial (RHBZ) relativistic Hartree-Bogoliubov models.

$A \approx 190$ mass region, where both prolate to oblate shape transitions as well as triaxial ground-state shapes have been predicted. An extensive analysis of this region has recently been performed using nonrelativistic Skyrme and Gogny interactions [18]. The self-consistent Hartree-Fock-Bogoliubov model has been used to study the evolution of the ground-state shapes of Yb, Hf, W, Os, and Pt isotopes. In particular, it has been shown that the isotopic chains with larger Z numbers in this mass region display a tendency toward triaxial shapes.

In this study we present the results of 3D RHB calculations of binding-energy maps for the sequence of even-A Pt isotopes with neutron numbers in the interval from $N = 106$ to $N = 126$. In Table I we list the calculated values of the β and γ deformation parameters for the absolute minima of the potential-energy surfaces (PES). One can follow the transition from the prolate deformed ^{186}Pt, through the region

of triaxially deformed $^{188-198}$Pt isotopes, to the slightly oblate ^{200}Pt, and finally to the spherical $^{202-204}$Pt isotopes. The ground-state β deformation steadily decreases as the number of neutrons increases and approaches the closed shell at $N = 126$. In order to analyze the nature of the shape transition in the Pt isotopic chain, in Fig. 7 we display the self-consistent RHB quadrupole binding-energy maps of the even-A $^{190-200}$Pt isotopes in the β-γ plane ($0^{\circ} \leqslant \gamma \leqslant 60^{\circ}$). All energies are normalized with respect to the binding energy of the absolute minimum, and the contours join points on the surface with the same energy. The PES of $^{190-198}$Pt are γ soft, with shallow minima at $\gamma \approx 30^{\circ}$. The nucleus ^{200}Pt displays a slightly oblate minimum, signaling the shell closure at $N = 126$.

As an illustrative example for the microscopic origin of the triaxial ground-state deformations, we consider the nucleus ^{192}Pt. The axially symmetric binding-energy curve of ^{192}Pt is plotted in the left panel of Fig. 8 (positive values of β correspond to prolate $\gamma = 0^{\circ}$, and negative β to oblate $\gamma = 60^{\circ}$ shapes). The plot in the panel on the right shows the binding-energy curve of ^{192}Pt at the fixed axial deformation $\beta = 0.18$, which corresponds to the position of the ground-state minimum, as a function of the triaxial deformation parameter γ. A well-developed triaxial minimum, calculated at $\gamma = 33^{\circ}$, has a depth of 0.8 MeV, whereas the oblate and prolate minima seen in the left panel are only saddle points in the β-γ plane.

The formation of deformed minima can be related to the occurrence of gaps or regions of low single-particle level density around the Fermi surface. In Figs. 9 and 10 we plot the

TABLE I. Calculated values of the β and γ deformation parameters for the absolute minima of the potential-energy surfaces (PES) of even-A Pt isotopes with $186 \leqslant A \leqslant 204$.

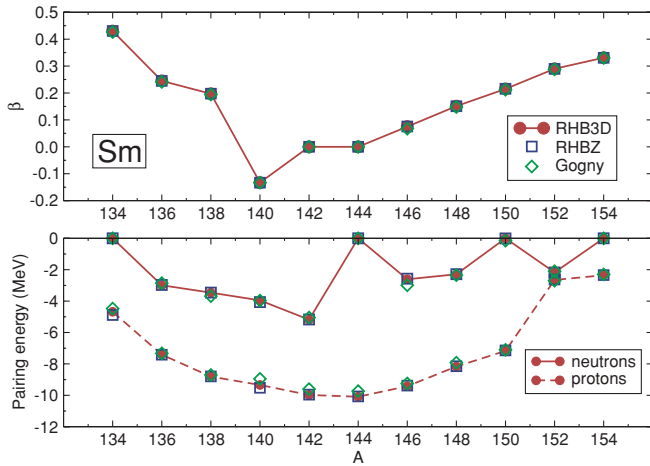| A	186	188	190	192	194	196	198	200	202	204
β	0.30	0.28	0.19	0.18	0.15	0.13	0.12	0.08	0	0
γ	0°	9°	34°	34°	34°	31°	33°	60°	0°	0°

FIG. 6. (Color online) 3D RHB (filled circles) and axial (RHBZ) (empty symbols) results for the self-consistent ground-state quadrupole deformations (upper panel), and neutron and proton pairing energies (lower panel) of even-A Sm isotopes. In calculations with axial symmetry both the separable force (squares) and the Gogny D1S force [5] (diamonds) are used.

proton and neutron single-particle energy levels in the canonical basis for ^{192}Pt. Solid curves denote levels with positive

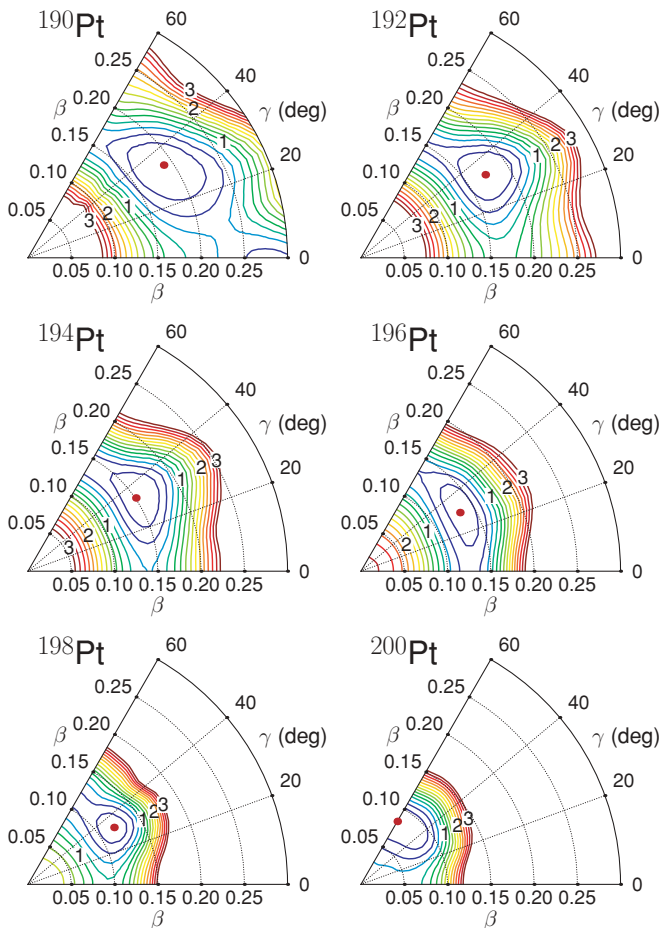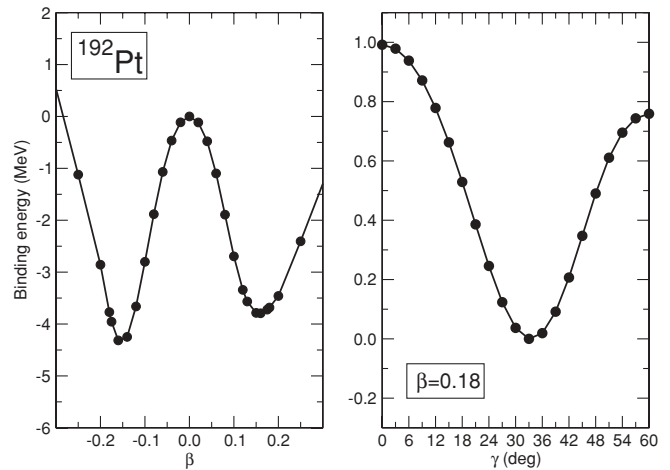FIG. 8. Left panel: Axially symmetric binding-energy curve of ^{192}Pt as a function of the deformation parameter β (positive values of β correspond to prolate $\gamma = 0°$ and negative β to oblate $\gamma = 60°$ shapes). Right panel: binding-energy curve of ^{192}Pt as a function of the triaxial deformation parameter γ. The axial deformation is held fixed at $\beta = 0.18$, which corresponds to the position of the ground-state minimum.

parity, and short-dashed curves levels with negative parity. The long-dashed (yellow) curve corresponds to the Fermi level. The leftmost and the rightmost panels display prolate and oblate axially symmetric single-particle levels, respectively, whereas the middle panel shows the single-particle levels as functions of γ for the fixed value of the axial deformation $|\beta| = 0.18$. This type of plot has been introduced in Ref. [19] to enable the identification of K quantum numbers of triaxial single-particle levels in the limits of axial symmetry at $\gamma = 0°$ and $\gamma = 60°$. In Fig. 9 we notice the occurrence of the gap between the proton

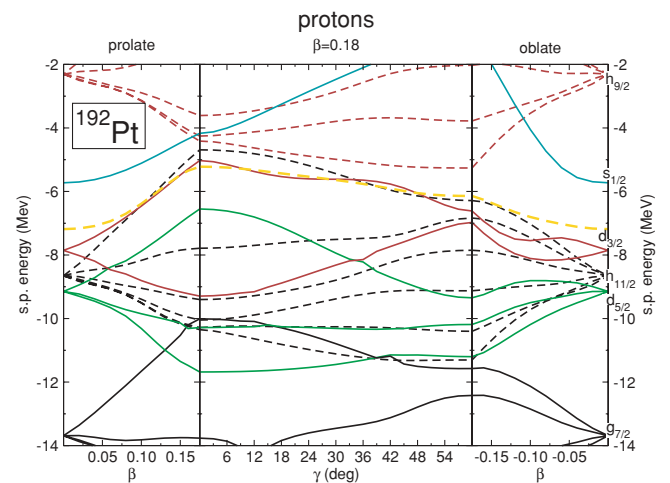FIG. 7. (Color online) Same as described in the caption to Fig. 1 but for the isotopes $^{190-200}$Pt.

FIG. 9. (Color online) Proton canonical single-particle energy levels of ^{192}Pt. Solid curves denote levels with positive parity and short-dashed curves levels with negative parity. The long-dashed (yellow) curve corresponds to the Fermi level. The leftmost and the rightmost panels display prolate and oblate axially symmetric single-particle levels, respectively. The middle panel shows the single-particle levels as functions of γ for the fixed value of the axial deformation $|\beta| = 0.18$.
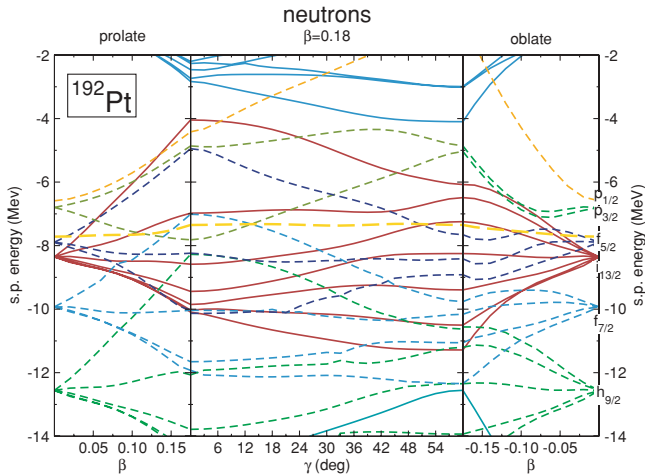
FIG. 10. (Color online) Same as described in the caption to Fig. 9 but for neutron single-particle levels.

single-particle levels in the vicinity of the Fermi surface around $\gamma = 30°$. The energy gap predominantly results from the down-sloping of one particular single-particle orbital, which originates from the spherical $d_{5/2}$ shell, as the deformation parameter γ increases from $\gamma = 0°$ to $\gamma = 60°$. This result is in agreement with the findings of Ref. [18]. The corresponding neutron single-particle levels, shown in Fig. 10, also display a region of low-level density around the Fermi surface at $\gamma \approx 30°$, although the gap is somewhat less pronounced in comparison to the proton gap. Finally, in Fig. 11 we plot the corresponding neutron and proton pairing energies as functions of the deformation parameter γ at the axial minimum $|\beta| = 0.18$. The decrease of the pairing energy reflects the low single-particle level density around the Fermi surface, which is the formation of gaps both for protons and neutrons.

IV. SUMMARY AND OUTLOOK

Realistic self-consistent mean-field calculations based on finite-range interactions, including exchange terms and/or
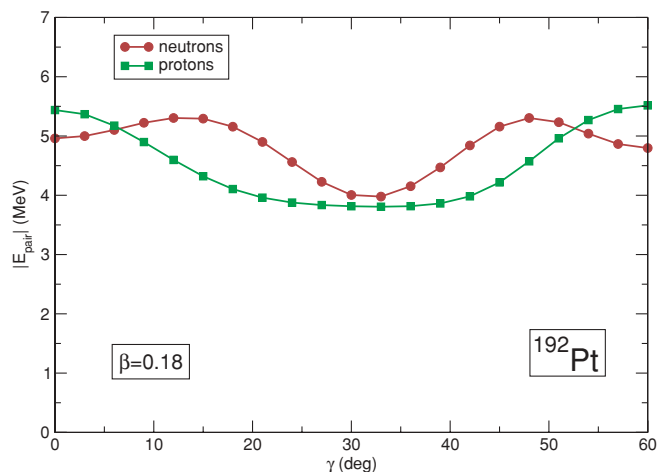

FIG. 11. Neutron and proton pairing energies in the ^{192}Pt nucleus as a function of the deformation parameter γ. The axial deformation parameter is fixed at $\beta = 0.18$, which corresponds to the position of the ground-state minimum.

pairing correlations, still present a considerable computational challenge [20–23], particularly if one considers complex triaxial shapes or extensions beyond the simplest mean-field approximation. A great advantage of mean-field models based on Skyrme-type zero-range interactions is that they provide a simple and elegant treatment of Fock exchange and pairing terms [24,25]. The disadvantage of such forces (i.e., the fact that they are constant in momentum space and can induce scattering of nucleons very high up into the continuum), does not appear at the Hartree or Hartree-Fock level, at which one considers only momenta up to the Fermi surface. In the pairing channel, however, because of the specific form of the BCS or Bogoliubov ansatz that takes into account pairing correlations on the mean-field level, ultraviolet divergencies occur for zero-range forces. One possible solution is the various cutoff procedures that have been used in the literature (cf. Ref. [26] and references therein). All these approximations, however, include additional nonphysical cutoff parameters. This is not a problem in calculations along the valley of beta stability, where gap parameters can be deduced from experimental masses. However, the use of cutoff parameters limits the predictive power of such models in unknown regions of the nuclear chart, such as for superheavy elements or very neutron-rich isotopes.

A completely different approach to the treatment of pairing correlations is the use of separable forces. A separable form of the pairing force for RHB calculations in finite nuclei has recently been introduced [8]. The force is separable in momentum space, and is completely determined by two parameters that are adjusted to reproduce the bell-shape curve of the pairing gap of the Gogny force in symmetric nuclear matter. Because of translational invariance, the pairing force is no longer exactly separable in coordinate space, but Talmi-Moshinsky techniques allow a simple transformation into a quickly converging series of separable terms in a harmonic-oscillator basis. Although different from the Gogny force, the corresponding effective pairing interaction has been shown to reproduce with high accuracy pairing gaps and energies calculated with the original Gogny force, both in spherical and axially deformed nuclei. In particular, this approach retains the basic advantage of the finite-range Gogny force (i.e., the natural cutoff in momentum space.

Applications have so far been restricted to the description of spherical [8] and axially deformed nuclei [10]. In this work we have extended the model to describe triaxially deformed nuclei. The numerical accuracy of the new model has been analyzed by comparing results with those obtained in axially symmetric calculations, using both the separable force as well as the original Gogny D1S force in the pairing channel.

To illustrate the applicability of this force in the description of realistic systems with possible triaxial deformations, we have explored the chain of even-A Sm nuclei ($Z = 62$) in the interval from ^{134}Sm to ^{156}Sm, and the sequence of Pt isotopes ($Z = 78$) ranging from ^{186}Pt to ^{204}Pt. For the magic neutron number $N = 82$ (i.e., for the ^{144}Sm isotope), a stable spherical minimum is found in the β-γ plane. The two neighboring nuclei ^{142}Sm and ^{146}Sm are still spherical, but with much softer energy surfaces. In heavier isotopes we find a rather rapid transition to prolate shapes with well-pronounced minima and increasing β deformation up to $\beta \approx 0.3$. In these heavier nuclei

we also find a soft saddle point on the oblate side that eventually becomes a shallow second minimum in the isotope ^{156}Sm. Decreasing the neutron number below the closed shell at $N = 82$, a γ-soft valley develops with increasing β deformation. For ^{140}Sm isotope we find a shallow oblate minimum, whereas for the lighter isotopes the minima are located on the prolate side, but the calculation predicts large fluctuations in the γ direction. In the case of Pt nuclei, starting with a prolate axially symmetric minimum at ^{186}Pt, we find an evolution of triaxial shapes in the isotopes $^{188-198}$Pt, with pronounced minima of the binding-energy maps close to $\gamma = 30°$. ^{200}Pt displays an oblate shape and, with decreasing β deformation, spherical shapes are predicted as the closed shell at $N = 126$ in ^{204}Pt is approached. The microscopic origin of the formation of triaxial minima has been illustrated in the example of ^{192}Pt.

One can envisage many possible applications of the separable pairing force. The force is simple enough to be applied in otherwise time-consuming calculations [e.g., description of triaxial effects, rotating nuclei, the fission process, and spherical and deformed quasiparticle random phase approximation (QRPA)]. It can also be used in various beyond mean-field extensions, such as restoration of broken symmetries, fluctuations of quadrupole moments, and particle-vibration coupling. In the current version of the model, the pairing force has been adjusted to the pairing gap of the phenomenological Gogny D1S force. However, one could also adjust the effective pairing force to a pairing gap in nuclear matter calculated in an *ab initio* approach [27], or even use a more sophisticated separable representation of the NN interaction [28].

APPENDIX A: THE SINGLE-NUCLEON BASIS

The Dirac single-nucleon spinors are expanded in the basis of eigenfunctions of a three-dimensional harmonic oscillator in Cartesian coordinates. In one dimension,

$$\phi_{n_\mu}(x_\mu) = b_\mu^{-1/2} \mathcal{N}_{n_\mu} H_{n_\mu}(\xi_\mu) e^{-\xi_\mu^2/2} \quad (\mu \equiv x, y, z), \quad (A1)$$

$\xi_\mu \equiv x_\mu/b_\mu$, and the oscillator length is defined as

$$b_\mu = \sqrt{\frac{\hbar}{m\omega_\mu}}. \quad (A2)$$

The normalization factor reads

$$\mathcal{N}_n = \pi^{-1/4}(2^n n!)^{-1/2}, \quad (A3)$$

and $H_n(\xi)$ denotes the Hermite polynomials [29]

$$\int_{-\infty}^{\infty} H_n(\xi)H_{n'}(\xi)e^{-\xi^2}d\xi = \delta_{nn'}. \quad (A4)$$

The basis state can be defined as the product of three HO wave functions (one for each dimension) and the spin factor:

$$\phi_\alpha(\mathbf{r}; m_s) = \phi_{n_x}(\xi_x)\phi_{n_y}(\xi_y)\phi_{n_z}(\xi_z)\chi_{m_s}, \quad (A5)$$

where the notation is $\alpha \equiv \{n_x, n_y, n_z\}$. For each combination of quantum numbers $\{n_x, n_y, n_z\}$, the spin part is chosen in such a way that the basis state is an eigenfunction of the x-simplex operator $\hat{S}_x = \hat{P}e^{-i\pi\hat{J}_x}$, where $\hat{P}$ denotes the parity operator. The positive and negative x-simplex operator eigenstates [30],

$$|n_x n_y n_z; i = +\rangle = |n_x n_y n_z\rangle \frac{i^{n_y}}{\sqrt{2}}[|\uparrow\rangle - (-1)^{n_x}|\downarrow\rangle], \quad (A6)$$

$$|n_x n_y n_z; i = -\rangle = |n_x n_y n_z\rangle(-1)^{n_x+n_y+1}$$
$$\times \frac{i^{n_y}}{\sqrt{2}}[|\uparrow\rangle + (-1)^{n_x}|\downarrow\rangle], \quad (A7)$$

are related by the time-reversal operator ($\hat{T} = i\sigma_y\hat{K}_0$)

$$|n_x n_y n_z; i = -\rangle = \hat{T}|n_x n_y n_z; i = +\rangle. \quad (A8)$$

For the Dirac spinor with a positive simplex eigenvalue, the large component corresponds to positive eigenvalues and the small component to negative eigenvalues,

$$\psi_i(\mathbf{r}, +) = \begin{pmatrix} f_i(\mathbf{r}, +) \\ i\,g_i(\mathbf{r}, -) \end{pmatrix}. \quad (A9)$$

The large and small components are expanded in terms of the basis states Eqs. (A6) and (A7),

$$f_i(\mathbf{r}; +) = \sum_\alpha^{\alpha_{\max}} f_i^\alpha \phi_\alpha(\mathbf{r}; +) \quad \text{and}$$

$$g_i(\mathbf{r}; -) = \sum_{\bar{\alpha}}^{\bar{\alpha}_{\max}} g_i^{\bar{\alpha}} \phi_{\bar{\alpha}}(\mathbf{r}; -). \quad (A10)$$

Positive simplex eigenstates are denoted by $|\alpha\rangle$ and negative simplex eigenstates by $|\bar{\alpha}\rangle$. If the basis states are arranged as $\{\alpha_1, \ldots, \alpha_M, \bar{\alpha}_1, \ldots \bar{\alpha}_M\}$, the x-simplex operator has a simple block-diagonal form, whereas the time-reversal operator is skew diagonal,

$$\hat{S}_x = i\begin{pmatrix} \mathbb{1} & 0 \\ 0 & -\mathbb{1} \end{pmatrix} \quad \text{and} \quad \hat{T} = \begin{pmatrix} 0 & \mathbb{1} \\ -\mathbb{1} & 0 \end{pmatrix}. \quad (A11)$$

If the dimension of each simplex block ($i = \pm$) is M, the dimension of the entire configuration space equals $2M$. In the present implementation of the model parity is also conserved, and this allows a further reduction of the basis to four simplex-parity blocks. For a given maximal number of oscillator shells $N_{\max}$, the dimension of the HO basis can be determined as follows. The states $|n_x n_y n_z\rangle$ within a major oscillator shell N are arranged as

n_x	n_y	n_z
0	0	N
0	1	$N-1$
$\vdots$	$\vdots$	$\vdots$
0	N	0
1	0	$N-1$
$\vdots$	$\vdots$	$\vdots$
1	$N-1$	0
N	0	0

and the number of 3D HO basis states in the shell N then reads

$$
\begin{aligned}
n_{\text{states}}(N) &= (N+1) + N + (N-1) + \cdots + 1 \\
&= \tfrac{1}{2}(N+1)(N+2). \quad \text{(A12)}
\end{aligned}
$$

Because parity is conserved, the basis can be separated into positive and negative parity blocks. The dimension of each block is determined by summing up the number of states in even-N or odd-N shells:

$$
\begin{aligned}
n_{\text{pos.}} &= \frac{1}{2} \sum_{k=0}^{k_{\text{max}}^+} (2k+1)(2k+2) \\
&= \frac{1}{6}(k_{\text{max}}^+ + 1)(k_{\text{max}}^+ + 2)(4k_{\text{max}}^+ + 3), \quad \text{(A13)}
\end{aligned}
$$

$$
\begin{aligned}
n_{\text{neg.}} &= \frac{1}{2} \sum_{k=0}^{k_{\text{max}}^-} (2k+2)(2k+3) \\
&= \frac{1}{6}(k_{\text{max}}^- + 1)(k_{\text{max}}^- + 2)(4k_{\text{max}}^- + 9), \quad \text{(A14)}
\end{aligned}
$$

where $k_{\text{max}}^+ = [N_{\text{max}}/2]$ and $k_{\text{max}}^- = [(N_{\text{max}} - 1)/2]$, and the square brackets denote integer division.

APPENDIX B: TRANSFORMATION OF THE PRODUCT OF 1D HO WAVE FUNCTIONS TO THE CENTER-OF-MASS FRAME

By multiplying the generating function for the Hermite polynomials

$$
g(x, p, b) = e^{2xp/b - p^2} = \sum_{n=0}^{\infty} \frac{1}{n!} p^n H_n(x/b), \quad \text{(B1)}
$$

with the factor $\frac{1}{\sqrt{b}} \pi^{-1/4} e^{-x^2/2b^2}$, we obtain the generating function for the HO wave functions:

$$
\frac{1}{\sqrt{b}} \pi^{-1/4} e^{-x^2/2b^2 + 2xp/b - p^2} = \sum_{n=0}^{\infty} \eta_n(p) \phi_n(x, b), \quad \text{(B2)}
$$

where $\eta_n(p)$ denotes

$$
\eta_n(p) = p^n \sqrt{\frac{2^n}{n!}}. \quad \text{(B3)}
$$

For the product of two generating functions

$$
\begin{aligned}
&g(x_1, p_1, b) g(x_2, p_2, b) \\
&= \frac{1}{b} \pi^{-1/2} e^{-\frac{1}{2b^2}(x_1^2 + x_2^2) + \frac{2}{b}(x_1 p_1 + x_2 p_2) - (p_1^2 + p_2^2)}, \quad \text{(B4)}
\end{aligned}
$$

a new set of coordinates is introduced,

$$
\left.\begin{aligned}
\tilde{x} &= \tfrac{1}{\sqrt{2}}(x_1 - x_2) \\
\tilde{X} &= \tfrac{1}{\sqrt{2}}(x_1 + x_2)
\end{aligned}\right\} \Longleftrightarrow
\begin{cases}
x_1 = \tfrac{1}{\sqrt{2}}(\tilde{X} + \tilde{x}) \\
x_2 = \tfrac{1}{\sqrt{2}}(\tilde{X} - \tilde{x})
\end{cases}, \quad \text{(B5)}
$$

with an analogous relation for the variables p_1 and p_2. The exponent in Eq. (B4) can now easily be expressed in terms of the new coordinates,

$$
\begin{aligned}
&g(x_1, p_1, b) g(x_2, p_2, b) \\
&= \frac{1}{b} \pi^{-1/2} e^{-\frac{1}{2b^2}(\tilde{x}^2 + \tilde{X}^2) + \frac{2}{b}(\tilde{x}\tilde{p} + \tilde{X}\tilde{P}) - (\tilde{p}^2 + \tilde{P}^2)} \\
&= g(\tilde{X}, \tilde{P}, b) g(\tilde{x}, \tilde{p}, b). \quad \text{(B6)}
\end{aligned}
$$

By using the definition of the generating functions

$$
\begin{aligned}
&g(\tilde{X}, \tilde{P}, b) g(\tilde{x}, \tilde{p}, b) \\
&= \sum_{N=0}^{\infty} \eta_N(\tilde{P}) \phi_N(\tilde{X}, b) \sum_{n=0}^{\infty} \eta_n(\tilde{p}) \phi_n(\tilde{x}, b), \quad \text{(B7)}
\end{aligned}
$$

the coefficients $\eta_N(\tilde{P})$ and $\eta_n(\tilde{p})$ can be expressed in terms of p_1 and p_2,

$$
\begin{aligned}
\eta_N(\tilde{P}) &= \sqrt{\frac{2^N}{N!}} \tilde{P}^N = \sqrt{\frac{1}{N!}}(p_2 + p_1)^N \\
&= \sqrt{\frac{1}{N!}} \sum_{M=0}^{N} \binom{N}{M} p_1^{N-M} p_2^M, \quad \text{(B8)}
\end{aligned}
$$

$$
\begin{aligned}
\eta_n(\tilde{p}) &= \sqrt{\frac{2^n}{n!}} \tilde{p}^n = \sqrt{\frac{1}{n!}}(p_1 - p_2)^n \\
&= \sqrt{\frac{1}{n!}} \sum_{m=0}^{n} (-1)^{n+m} \binom{n}{m} p_1^m p_2^{n-m}. \quad \text{(B9)}
\end{aligned}
$$

The product of generating functions Eq. (B7) then reads

$$
\begin{aligned}
&\sum_{n,N=0}^{\infty} \phi_N(\tilde{X}, b) \phi_n(\tilde{x}, b) \sqrt{\frac{1}{N!n!}} \sum_{M=0}^{N} \sum_{m=0}^{n} (-1)^{n+m} \\
&\times \binom{N}{M} \binom{n}{m} p_1^{N-M+m} p_2^{M+n-m}. \quad \text{(B10)}
\end{aligned}
$$

With the introduction of the auxiliary indices,

$$
n_1 = N - M + m \quad \text{and} \quad n_2 = M + n - m, \quad \text{(B11)}
$$

the product Eq. (B10) can be rewritten in the form

$$
\begin{aligned}
&g(\tilde{X}, \tilde{P}, b) g(\tilde{x}, \tilde{p}, b) \\
&= \sum_{n_1,n_2=0}^{\infty} p_1^{n_1} p_2^{n_2} \sum_{n,N=0}^{\infty} \phi_N(\tilde{X}, b) \phi_n(\tilde{x}, b) \sqrt{\frac{1}{N!n!}} \\
&\times \sum_{M=0}^{N} \sum_{m=0}^{n} (-1)^{n+m} \binom{N}{M} \binom{n}{m} \delta_{n_1, N-M+m} \delta_{n_2, M+n-m}. \\
&\quad \text{(B12)}
\end{aligned}
$$

One of the Kronecker symbols can be used to eliminate the sum over M,

$$
\begin{aligned}
&g(\tilde{X}, \tilde{P}, b)g(\tilde{x}, \tilde{p}, b) \\
&= \sum_{n_1,n_2=0}^{\infty} p_1^{n_1} p_2^{n_2} \sum_{n,N=0}^{\infty} \phi_N(\tilde{X}, b)\phi_n(\tilde{x}, b)\sqrt{\frac{1}{N!n!}}\delta_{n_1+n_2,N+n} \\
&\quad \times \sum_{m=0}^{n} (-1)^{n+m} \binom{N}{N-n_1+m}\binom{n}{m}.
\end{aligned}
\tag{B13}
$$

A comparison with the equivalent relation for the product [cf. Eq. (B4)]

$$
\begin{aligned}
&g(x_1, p_1, b)g(x_2, p_2, b) \\
&= \sum_{n_1,n_2=0}^{\infty} p_1^{n_1} p_2^{n_2} \sqrt{\frac{2^{n_1+n_2}}{n_1!n_2!}}\phi_{n_1}(x_1, b)\phi_{n_2}(x_2, b), \quad \text{(B14)}
\end{aligned}
$$

leads to the final expression for the transformation of the product of 1D HO wave functions,

$$
\phi_{n_1}(x_1, b)\phi_{n_2}(x_2, b) = \sum_{N,n} M_{n_1 n_2}^{nN}\phi_N(\tilde{X}, b)\phi_n(\tilde{x}, b), \quad \text{(B15)}
$$

where $M_{n_1 n_2}^{nN}$ are the 1D Talmi-Moshinsky brackets [31–33]:

$$
\begin{aligned}
M_{n_1 n_2}^{nN} &= \sqrt{\frac{n_1!n_2!}{n!N!}}\sqrt{\frac{1}{2^{N+n}}}\delta_{n_1+n_2,n+N}\sum_{m}(-1)^{n+m} \\
&\quad \times \binom{N}{N-n_1+m}\binom{n}{m}.
\end{aligned}
\tag{B16}
$$

For the calculation of matrix elements of the pairing interaction, the center of mass and relative coordinates are used,

$$
X \equiv \frac{1}{2}(x_1 + x_2) = \frac{1}{\sqrt{2}}\tilde{X} \quad \text{and} \quad x \equiv x_1 - x_2 = \sqrt{2}\tilde{x}.
\tag{B17}
$$

The HO wave functions are expressed in terms of X and x,

$$
\begin{aligned}
\phi_N(\tilde{X}, b) &= \phi_N(\sqrt{2}X, b) = \frac{1}{\sqrt{b}}\mathcal{N}_n H_n(\sqrt{2}X/b)e^{-2x^2/2b^2} \\
&= \frac{1}{\sqrt{2}}\phi_N(X, B),
\end{aligned}
\tag{B18}
$$

$$
\begin{aligned}
\phi_n(\tilde{x}, b) &= \phi_n(x/\sqrt{2}, b) = \frac{1}{\sqrt{b}}\mathcal{N}_n H_n(x/\sqrt{2}b)e^{-x^2/4b^2} \\
&= \sqrt{2}\phi_n(x, b_r),
\end{aligned}
\tag{B19}
$$

where we have defined the oscillator lengths $B = b/\sqrt{2}$ and $b_r = \sqrt{2}b$. Finally, the product of two HO wave functions expressed in terms of the center-of-mass and relative coordinates reads

$$
\phi_{n_1}(x_1, b)\phi_{n_2}(x_2, b) = \sum_{N,n} M_{n_1 n_2}^{nN}\phi_N(X, B)\phi_n(x, b_r). \quad \text{(B20)}
$$

APPENDIX C: CALCULATION OF PAIRING MATRIX ELEMENTS

The antisymmetric matrix elements of the pairing interaction Eq. (19) can be separated into a product of spin and coordinate space factors

$$
\langle\alpha\bar{\beta}|V|\gamma\bar{\delta}\rangle_a = \langle\alpha\bar{\beta}|W\tfrac{1}{2}(1 - P^\sigma)|\gamma\bar{\delta}\rangle_a. \tag{C1}
$$

The operator $\frac{1}{2}(1 - P^\sigma)$ projects onto the $S = 0$ spin-singlet product state

$$
\begin{aligned}
|\gamma\bar{\delta}\rangle_{S=0} = -|\bar{\delta}\gamma\rangle_{S=0} &= \tfrac{1}{2}i^{n_y^\gamma + n_y^\delta}(-1)^{n_y^\delta + 1} \\
&\times \delta_{n_x^\gamma + n_x^\delta,\text{even}}[|\uparrow\downarrow\rangle - |\downarrow\uparrow\rangle]|n^\gamma n^\delta\rangle, \quad \text{(C2)}
\end{aligned}
$$

and the problem is reduced to the calculation of the spatial part of the matrix element

$$
\begin{aligned}
\langle\alpha\bar{\beta}|V|\gamma\bar{\delta}\rangle_a &= (-i)^{n_y^\alpha - n_y^\beta}\delta_{n_x^\alpha + n_x^\beta,\text{even}}i^{n_y^\gamma - n_y^\delta} \\
&\times \delta_{n_x^\gamma + n_x^\delta,\text{even}}\langle n^\alpha n^\beta|W|n^\gamma n^\delta 1\rangle. \quad \text{(C3)}
\end{aligned}
$$

For $W(\boldsymbol{r}_1, \boldsymbol{r}_2, \boldsymbol{r}_1', \boldsymbol{r}_2') = G\delta\left(\boldsymbol{R} - \boldsymbol{R}'\right)P(\boldsymbol{r})P(\boldsymbol{r}')$ [cf. Eq. (17)], the spatial part of the matrix element

$$
\begin{aligned}
\langle n^\alpha n^\beta|W|n^\gamma n^\delta\rangle &\equiv \int \phi_{n_\alpha}(\boldsymbol{r}_1)\phi_{n_\gamma}(\boldsymbol{r}_2)W(\boldsymbol{r}_1, \boldsymbol{r}_2, \boldsymbol{r}_1', \boldsymbol{r}_2') \\
&\times \phi_{n_\beta}(\boldsymbol{r}_1')\phi_{n_\delta}(\boldsymbol{r}_2')d^3r_1 d^3r_2 d^3r_1' d^3r_2' \quad \text{(C4)}
\end{aligned}
$$

can be decomposed into three Cartesian components

$$
\langle n^\alpha n^\beta|W|n^\gamma n^\delta\rangle = G W_x W_y W_z. \tag{C5}
$$

Here we only derive a detailed expression for the x component

$$
\begin{aligned}
W_x &= \int \phi_{n_x^\alpha}(x_1, b_x)\phi_{n_x^\beta}(x_2, b_x)P(x)\delta(X - X')P(x') \\
&\times \phi_{n_x^\gamma}(x_1', b_x)\phi_{n_x^\delta}(x_2', b_x)dx_1 dx_2 dx_1' dx_2'. \quad \text{(C6)}
\end{aligned}
$$

By transforming to the center of mass and relative coordinates Eq. (B17), and making use of the 1D Talmi-Moshinsky transformation Eq. (B20), the integrals over the center-of-mass coordinates X and X' are solved analytically, and we find

$$
W_x = \sum_{N_x} M_{n_x^\alpha n_x^\beta}^{n_x N_x} I_{n_x}(b_x)M_{n_x^\beta n_x^\delta}^{n_x' N_x}I_{n_x'}(b_x), \tag{C7}
$$

where the selection rules

$$
n_\alpha^x + n_\beta^x = n_x + N_x \quad \text{and} \quad n_\gamma^x + n_\delta^x = n_x' + N_x'. \tag{C8}
$$

have been used to eliminate the sums over n_x and n_x'. $I_{n_x}(b_x)$ reads

$$
I_{n_x}(b_x) = \int P(x)\phi_{n_x}(x, b_{x,r})dx. \tag{C9}
$$

To evaluate this integral, we make use of the generating function for the HO wave functions Eq. (B2), and calculate the following expression:

$$
\begin{aligned}
J(p, b) &= \int_{-\infty}^{\infty} g(x, p, b)P(x)dx \\
&= \pi^{-1/4}\sqrt{\frac{b}{b^2 + 2a^2}}\sum_{n=0}^{\infty}(-1)^n\left(\frac{b^2 - 2a^2}{b^2 + 2a^2}\right)^n p^{2n}.
\end{aligned}
\tag{C10}
$$

Using the definition of the generating function Eq. (B2), this integral can also be written as follows:

$$J(p, b) = \sum_{n=0}^{\infty} p^{2n} \sqrt{\frac{2^{2n}}{(2n)!}} \int_{-\infty}^{\infty} P(x)\phi_{2n}(x, b). \quad (C11)$$

The series contains only even powers because $P(x)$ is a symmetric function. By comparing Eqs. (C10) and (C11), we obtain

$$\int_{-\infty}^{\infty} P(x)\phi_n(x, b) = \pi^{-1/4}\sqrt{\frac{b}{b^2 + 2a^2}}(-1)^{n/2}$$
$$\times \left(\frac{b^2 - 2a^2}{b^2 + 2a^2}\right)^{n/2} \delta_{n,\text{even}}, \quad (C12)$$

and finally, inserting the relative oscillator length $b_r = \sqrt{2}b$ (cf. Appendix B),

$$I_n(b) = \frac{1}{(2\pi)^{1/4}}\sqrt{\frac{b}{b^2 + a^2}}(-1)^{n/2}\left(\frac{b^2 - a^2}{b^2 + a^2}\right)^{n/2} \delta_{n,\text{even}}. \quad (C13)$$

To summarize, we find that the antisymmetrized matrix element of the pairing interaction Eq. (19),

$$\langle \alpha\bar{\beta}|V|\gamma\bar{\delta}\rangle_a = G \sum_{N_x=0}^{N_x^0} \sum_{N_y=0}^{N_y^0} \sum_{N_z=0}^{N_z^0} \left(V_{\alpha\bar{\beta}}^{N_x N_y N_z}\right)^* V_{\gamma\bar{\delta}}^{N_x N_y N_z}, \quad (C14)$$

can be represented as a sum of separable terms in a 3D Cartesian HO basis, with the single-particle matrix elements

$$V_{\alpha\bar{\beta}}^{N_x N_y N_z} = \delta_{n_x^\alpha + n_x^\beta,\text{even}} i^{n_y^\alpha - n_y^\beta} V_{n_x^\alpha n_x^\beta}^{N_x}(b_x) V_{n_y^\alpha n_y^\beta}^{N_y}(b_y) V_{n_z^\alpha n_z^\beta}^{N_z}(b_z). \quad (C15)$$

The factors $V_{n_1 n_2}^{nN}(b)$ are given by

$$V_{n_1 n_2}^{N}(b) = M_{n_1 n_2}^{nN} I_n(b) \quad \text{with} \quad n = N - n_1 - n_2. \quad (C16)$$

The Talmi-Moshinsky brackets $M_{n_\alpha n_\beta}^{nN}$ are defined in Eq. (B16), and the integrals $I_n(b)$ are given in Eq. (C13).

[1] M. Bender, P.-H. Heenen, and P.-G. Reinhard, Rev. Mod. Phys. **75**, 121 (2003).

[2] D. Vretenar, A. V. Afanasjev, G. A. Lalazissis, and P. Ring, Phys. Rep. **409**, 101 (2005).

[3] P. Ring, Prog. Part. Nucl. Phys. **37**, 193 (1996).

[4] J. F. Berger, M. Girod, and D. Gogny, Nucl. Phys. A **428**, 23c (1984).

[5] J. F. Berger, M. Girod, and D. Gogny, Comput. Phys. Commun. **63**, 365 (1991).

[6] J. Meng, Nucl. Phys. A **635**, 3 (1998).

[7] T. Nikšić, P. Ring, and D. Vretenar, Phys. Rev. C **71**, 044320 (2005).

[8] Y. Tian, Z. Y. Ma, and P. Ring, Phys. Lett. B **676**, 44 (2009).

[9] Y. Tian, Z. Y. Ma, and P. Ring, Phys. Rev. C **79**, 064301 (2009).

[10] Y. Tian, Z. Y. Ma, and P. Ring, Phys. Rev. C **80**, 024313 (2009).

[11] T. Nikšić, Z. P. Li, D. Vretenar, L. Próchniak, J. Meng, and P. Ring, Phys. Rev. C **79**, 034303 (2009).

[12] M. Serra and P. Ring, Phys. Rev. C **65**, 064324 (2002).

[13] G. A. Lalazissis, T. Nikšić, D. Vretenar, and P. Ring, Phys. Rev. C **71**, 024312 (2005).

[14] N. Paar, D. Vretenar, E. Khan, and G. Coló, Rep. Prog. Phys. **70**, 691 (2007).

[15] P. Ring and P. Schuck, *The Nuclear Many-Body Problem* (Springer, Berlin, 1980).

[16] G. A. Lalazissis, D. Vretenar, P. Ring, M. Stoitsov, and L. Robledo, Phys. Rev. C **60**, 014310 (1999).

[17] G. Audi, A. H. Wapstra, and C. Thibault, Nucl. Phys. A **729**, 337 (2003).

[18] L. M. Robledo, R. Rodríguez-Guzmán, and P. Sarriguren, J. Phys. G **36**, 115104 (2009).

[19] S. Ćwiok, P.-H. Heenen, and W. Nazarewicz, Nature (London) **433**, 705 (2005).

[20] J.-P. Delaroche, M. Girod, H. Goutte, and J. Libert, Nucl. Phys. A **771**, 103 (2006).

[21] N. Schunck and J. L. Egido, Phys. Rev. C **78**, 064305 (2008).

[22] S. Hilaire and M. Girod, Eur. Phys. J. A **33**, 237 (2007).

[23] W. Long, P. Ring, N. Van Giai, and J. Meng, Phys. Rev. C **81**, 024308 (2010).

[24] D. Vautherin and D. M. Brink, Phys. Rev. C **5**, 626 (1972).

[25] J. Dobaczewski, H. Flocard, and J. Treiner, Nucl. Phys. A **422**, 103 (1984).

[26] S. Karatzikos, A. V. Afanasjev, G. A. Lalazissis, and P. Ring, Phys. Lett. B **689**, 72 (2010).

[27] S. Gandolfi, A. Y. Illarionov, S. Fantoni, F. Pederiva, and K. E. Schmidt, Phys. Rev. Lett. **101**, 132501 (2009).

[28] T. Duguet and T. Lesinski, Eur. Phys. J. ST **156**, 207 (2008).

[29] *Handbook of Mathematical Functions*, edited by M. Abramowitz and I. A. Stegun (Dover, New York, 1970).

[30] J. Peng, J. Meng, P. Ring, and S. Q. Zhang, Phys. Rev. C **78**, 024313 (2008).

[31] I. Talmi, Helv. Phys. Acta **25**, 185 (1952).

[32] M. Moshinsky, Nucl. Phys. **13**, 104 (1959).

[33] L. Chaos-Cador and E. Ley-Koo, Int. J. Quantum Chem. **97**, 844 (2004).